Co-published by
Institute of Fluid-Flow Machinery
Polish Academy of Sciences
Committee on Thermodynamics and Combustion
Polish Academy of Sciences

http://www.imp.gda.pl/archives-of-thermodynamics/

Comprehensive optimization of a novel thermo-hydraulic machine for mechanical power generation

Asmaa Guelib[a], Djallel Zebbar[b*], Zakaria Rahmani[b], Souhila Zebbar[b], Kouider Mostefa[b], Sahraoui Kherris[b], Said Mekroussi[a]

[a]Research Laboratory of Industrial Technologies, Departmentof Mechanical Engineering, Faculty of Applied Sciences, Ibn Khaldoun University, B.P. 78 Zaâroura 14000 Tiaret, Algeria
[b]Laboratory of Mechanical Engineering, Materials and Structures, Faculty of Sciences and Technology, Tissemsilt University – Ahmed ben Yahia Elwancharissi, Benhamouda B.P 182, 38010 Tissemsilt, Algeria
*Corresponding author email: djallel.zebbar@univ-tissemsilt.dz

Received: 08.07.2024; revised: 05.10.2024; accepted: 05.01.2025

Abstract

This paper is dedicated to the multi-aspect optimization of a novel thermo-hydraulic machine with liquid piston operating according to organic Rankine cycle, designed for mechanical power generation from low temperature reservoirs. This involves the implementation of thermodynamic and hydraulic analyses. Several issues have been identified in thermo-hydraulic machines built to date, particularly the limitation imposed by the location of the expansion phase under the equilibrium dome, which constrains maximum output work. This issue is addressed through the application of steam superheating followed by the organic Rankine cycle. The thermodynamic analysis showed that the R1233zd is the most suitable working fluid for the suggested novel machine within the temperature range of 65−130°C. The selection of the best working fluid was followed by the dimensioning of the hydraulic part of the machine under optimal operating conditions. A new parameter was introduced to link the gas and hydraulic sides of the machine. It is about the time scale of the cycle which influences significantly the mechanical output power. Furthermore, mathematical modelling of the hydraulic part of the machine concludes that high mechanical power output can only be achieved only in modes of operation with high thermal efficiencies. Conversely, operational modes with high second law efficiencies fail to deliver high mechanical power levels. These two conclusions can be regarded as equivalent to the various postulates of the second law of thermodynamics.

Keywords: Thermo-hydraulic machine; Organic Rankine cycle; Liquid piston; Mechanical power generation

Vol. 46(2025), No. 1, 25–36; doi: 10.24425/ather.2025.154178

Cite this manuscript as: Guelib, A., Zebbar, D., Rahmani, Z., Zebbar, S., Mostefa, K., Kherris, S., & Mekroussi, S. (2025). Comprehensive optimization of a novel thermo-hydraulic machine for mechanical power generation. *Archives of Thermodynamics*, 46(1), 25–36.

1. Introduction

Fossil fuels, including coal, oil, and gas, have served as the backbone of the global energy supply for the past century. However, since the beginning of the twenty-first century, their extensive use is increasingly recognised as unsustainable due to several significant issues. Foremost among these are their environmental impacts. Large quantities of greenhouse gases, particularly carbon dioxide (CO_2), are released through the combustion of fossil fuels, contributing significantly to global warming and climate change. Another critical issue is the non-renewable nature of fossil fuels, which presents inherent limitations [1].

Nomenclature

d – diameter of the hydraulic pipe, m
D – diameter of the transfer cylinder, m
f – frequency, 1/s
g – gravitational acceleration, m/s^2
GWP – global warming potential
h – specific enthalpy, J/kg
H – height, m
K – flow coefficient, m^3/s
$\dot{m}$ – mass flow rate of the cycle, kg/s
ODP – ozone depletion potential
P – power, W
p – pressure, Pa
Q – specific heat exchanged during transformation, J/kg
Re – Reynolds number
T – temperature, K
v – specific volume, m^3/kg
$\dot{V}$ – flow rate, m^3/s
V – velocity, m/s
W – specific work, J/kg
y – extraction ratio

Greek symbols

ΔH – height difference, m
Δp – pressure difference, Pa
η – efficiency
v – specific volume, m^3/kg
ρ – density of the fluid, kg/m^3
σ – kinematic viscosity, m^2/s
τ – duration of a thermodynamic cycle, s

Subscripts and Superscripts

cond – condenser
evap – evaporator
exp – expansion
h – height
hyd – hydraulic
in – inlet
II – second
l – low
LT – work-transfer liquid
max – maximal
min – minimal
opt – optimal
sc – superheated
th – thermal
vs – valves

Abbreviations and Acronyms

CAPILI – Carnot with piston liquid
CT, CT' – transfer cylinders
FLP – pressurized fluid of liquid piston
ORC – organic Rankine cycle
ORPILI – organic Rankine cycle with liquid piston
OTEC – ocean thermal energy conversion

The widespread adoption of non-conventional energy sources and technologies to reduce reliance on fossil fuels has been driven by the pursuit of a sustainable and clean environment [2]. These energy sources, known as renewable energy sources, offer numerous advantages beyond their economic and social benefits. They encompass solar, wind, geothermal, biomass, and ocean thermal energy.

Solar energy, including both thermal solar energy and photovoltaic (solar electrical), stands out as one of Earth's major available energy sources compared to other forms. Its utilization spans a long history of applications in residential, vehicular, aerospace and naval sectors [3]. Wind energy is another significant player in the global energy market, representing a substantial and growing sector in renewable energy production [4].

Geothermal energy taps into the Earth's internal heat. Beneath the Earth's crust lies a layer of dense, molten rock that often contains water reservoirs, occasionally surfacing as hot springs. When not naturally accessible, this heated water can be extracted through drilling. It serves as a virtually cost-free energy source, whether used directly as hot water, steam, or heat, or to generate electricity [5].

Biomass energy, also known as bioenergy, derives from the conversion of biomass into various forms of energy such as electricity, heat, power, or transportation fuels. Biomass qualifies as a renewable energy source due to its ability to cultivate, harvest, and regenerate trees and plants within short timeframes. Additionally, this process consistently yields residues, wastes, and gases [6].

In addition, ocean thermal energy has gained significant recognition over the past decade as a renewable energy source for sustainable energy production systems. Ocean thermal energy conversion (OTEC) technology harnesses clean power from the natural thermal gradient between different layers of seawater. This temperature gradient is considered a self-replenishing energy source [3], driven by natural processes within the ocean.

Low-temperature energies, including industrial waste heat, low-temperature geothermal energy, and solar thermal energy, present promising solutions for enhancing energy efficiency and sustainability [7]. Power generation plays a crucial role in utilizing and recycling these low-temperature heat sources [8]. Thermo-hydraulic energy conversion systems, which transform thermal energy into hydraulic or mechanical energy, are increasingly gaining attention for their potential applications in both power generation and industrial processes. These systems are particularly suitable for generating mechanical power from low-temperature heat reservoirs such as solar and geothermal sources.

Consideration should be given to thermo-hydraulic conversion systems, such as those employing liquid piston technology to generate power. Liquid pistons are devices that utilize a liquid to produce mechanical movement or perform work, a concept pioneered by Humphrey in 1909 [9]. Humphrey later advanced this technology by developing an internal combustion engine based on the Atkinson cycle, which found extensive use in pumping stations and irrigation applications.

Liquid piston technology has undergone significant evolution and has found application across various fields and systems.

Van de Ven et al. [10] advocated for the liquid piston concept as a solution to challenges encountered in designing fluid engines and Stirling pumps. This concept is also integral to the operation of steam and refrigeration machines [11–13].

The thermo-hydraulic process CAPILI (Carnot with piston liquid) illustrates the application of liquid piston technology, marking significant advancements in renewable energy. This technology has been successfully utilized in OTEC power production [14], as well as in residential applications [15]. This thermo-hydraulic process can operate either in engine mode, where the evaporator temperature is higher than the condenser temperature (used for cogeneration or electricity production), or in receiver mode, where the evaporator temperature is lower than the condenser temperature (employed for heat pump or refrigeration purposes) [16]. The CAPILI process, whether configured as an engine or heat pump, is designed in two primary configurations: the "1st type" or the "2nd type," corresponding to these operational modes. The 2nd type CAPILI process closely adheres to the Carnot cycle, while the 1st type CAPILI process exhibits slight deviations [15].

The CAPILI engine typically comprises two cylinders connected to separate heat exchangers (evaporator and condenser), operating at different pressures. The transfer of work between the machine and its surroundings is facilitated by a hydraulic/mechanical converter, through which a liquid circulates alternately between the evaporator and the condenser during the isothermal phases of the cycle [16]. The work-transfer liquid (LT) in the CAPILI machine is required to have a very low saturation pressure (such as oil) at the process operating temperatures and must be immiscible with, and ideally denser than, the working fluid [15]. The working fluids used in these machines include pure substances or azeotropic mixtures (such as hydrocarbons, hydrofluorocarbons (HFCs), H_2O, etc.), which closely approximate or mimic the Carnot cycle (motor or receiver).

For a comprehensive understanding of the current study, it is essential to review previous research conducted on the CAPILI thermo-hydraulic machine. This process has been extensively investigated in several prior studies [14–19]. Semmari et al. [14] extensively examined the CAPILI process, investigating its performance, selecting appropriate working fluids, and developing dynamic models to simulate its behavior within OTEC power plants. Mauran et al. [15] presented the thermo-hydraulic CAPILI process with the primary objective of achieving optimal efficiency. They conducted a comprehensive analysis of thermodynamic cycles, explored various applications such as trigeneration, and assessed the system's performance and sustainability advantages. Additionally, the same authors [15] emphasized the potential of the CAPILI system to enhance energy efficiency and reduce greenhouse gas emissions in both residential and commercial sectors. Stitou [16] provided a comprehensive analysis of the CAPILI thermo-hydraulic process, offering analytical tools and effective solutions for examining the transformation and conversion of thermal energy through thermo-hydraulic processes. Borgogno et al. [17] investigated the application of the CAPILI process in trigeneration for residential areas, while Semmari et al. [18] conducted experimental validation of an innovative analytical model for a thermo-hydraulic CAPILI system designed for re-sidential use, emphasizing hydraulic resistance as a foundational concept. Zebbar et al. [19] conducted a thermodynamic analysis of a machine operating under the first type of CAPILI cycle, designed to convert low-grade heat sources such as solar and geothermal energy into mechanical power. They identified n-butane (R-600) as the optimal working fluid, achieving peak thermal efficiencies of 20.3%, Carnot efficiencies of 23%, and second law efficiencies of 88% at specific operating temperatures of 30°C for the condenser and 120°C for the evaporator.

This brief review encompassed renewable energy sources for sustainable environments, previous studies on liquid pistons, and the thermo-hydraulic CAPILI process. It has highlighted several shortcomings in the current CAPILI machine.

In the previous research on the CAPILI thermo-hydraulic process, the working fluid undergoes continuous state changes, alternating between liquid and vapour phases. A significant challenge involves compressing a two-phase mixture or extracting work from an isentropic two-phase expansion [20]. The liquid piston plays a crucial role in overcoming this challenge, enabling the CAPILI cycle to operate without the necessity for superheating or subcooling the working fluid prior to expansion or compression. Consequently, thermodynamic irreversibilities are minimized in CAPILI cycles, leading to an enhanced overall efficiency of the cycle [20]. Furthermore, the patent of the Research Laboratory in Engineering, Materials and Structures [21], filed in March 2022 at the Algerian National Institute of Industrial Property (*Institut National Algérien de la Propriété Industrielle*), identified a critical issue with the CAPILI cycle related to the location of the expansion phase under the equilibrium dome. This positioning maintains the maximum temperature in the cycle significantly above the critical temperature of the working fluid, thereby restricting the maximum output work or mechanical power per unit mass of the working fluid. Moreover, in the same patent [21], it is reported that the CAPILI machine depends on a very complex control system consisting of several solenoid valves and sensors to reverse the direction of flow in the hydraulic motor and finally, the existing thermo-hydraulic CAPILI machine has a condensate transfer pump driven by an electric motor, which is far from practical.

The issues mentioned above were addressed in the Research Laboratory in Engineering, Materials and Structures patent [21] through several advancements. Firstly, steam superheating was introduced to raise the average temperature of heat input within the cycle, transitioning it into an organic Rankine cycle variant known as ORPILI (organic Rankine with piston liquid). Secondly, the proposed novel configuration of the ORPILI thermo-hydraulic machine reduced the number of solenoid valves by implementing a mechanical transmission. Thirdly, a steam turbine was integrated to drive the transfer pump, enhancing the efficiency and performance of the system.

This study aims to argue in favour of the novel ORPILI machine through thermo-hydraulic analysis. The primary objective is to increase the specific mechanical work output (or mechanical power) of the thermo-hydraulic machine while maintaining efficiencies similar to those of the CAPILI cycle. This enhancement is made possible by integrating a steam superheater, which

allows for an increase in the average temperature of the heat input into the cycle. Hence, the move to the organic Rankine cycle with superheating.

Therefore, the following objectives are set for this study:

- Develop a comprehensive thermodynamic model and analysis for the proposed ORPILI cycle.
- Evaluate the performance of the ORPILI cycle using different working fluids (e.g. R600a, R600, R1234ze, R1234yf, R1233zd, and SESE36).
- Dimension the hydraulic components of the proposed machine according to the input thermal power.

These objectives are crucial for substantiating the efficiency and feasibility of the ORPILI machine, as discussed earlier.

This paper is structured as follows: first, a description of the novel configuration of the thermo-hydraulic machine is presented in Section 2. A thermodynamic analysis is discussed in Section 3, followed by the results and discussion in Section 4. Section 5 provides the hydraulic analysis, with the main findings discussed in Section 6. Finally, concluding remarks are presented in Section 7.

2. Description of the novel concept of the organic Rankine thermo-hydraulic machine with liquid piston

2.1. Structure

The component layout of the proposed thermo-hydraulic system is illustrated in Fig. 1. The system consists of an evaporator (3) connected to the heat source at the high-temperature, $T_{evap} = T_h$, a condenser (4) connected to the heat sink at the low-temperature, $T_{cond} = T_l$, two insulated work-transfer cylinders (1) and (19), steam turbine (5), a transfer pump (6) driven by superheated steam for transferring the condensate to the evaporator, and to maintain the pressure difference or drop between the evaporator and the condenser ($\Delta p = p_{evap} - p_{cond}$), a superheatter (2), two hydraulic motors (7) and (8) coupled through a pair of gears (9) and (11), a generator (10), a 2-way solenoid valve (12) and (13), an extraction steam valve (14), four non-return valves (15)−(18) and level sensors (20) and (21).

2.2. Principle of operation

The novel thermo-hydraulic machine presented in this work operates as follows: heat is introduced in the evaporator (3), where the working fluid evaporates and proceeds into the superheater (2). Then, the steam passes through the solenoid valve (12) and enters the work-transfer cylinder (19). The steam acts on the surface of the liquid which plays the role of liquid piston. It is possible to insert a movable wall such as a diaphragm between the liquid and the steam to avoid their direct contact. The pressurized fluid of the liquid piston (FLP) passes into the hydraulic motor (7), which is coupled to a generator (10) via a freewheel. The FLP then moves to the work-transfer cylinder (1) through the non-return valve (16). During this phase, the solenoid valve (13) connects the steam space in the work transfer cylinder (1) with the condenser (4) at a pressure p_{cond}. The condensate in the condenser (4) is pumped to the evaporator (3) by pump (6), which is driven by the steam turbine (5). The steam turbine (5) is supplied from the superheater (2) through the extraction valve (14). In addition to transferring the condensate, the pump maintains the pressure drop between the evaporator and the condenser ($\Delta p = p_{evap} - p_{cond}$). When the free level of FLP reaches the designated level detected by the level sensor (20), the non-return valves (16) and (18) are activated to change the direction of flows. In this case, the superheated steam passes into the work transfer cylinder (1). The pressure created by the steam above the surface of the liquid piston returns the hydraulic oil to the hydraulic motor (8) through the non-return valve (16). The hydraulic motor (8) is coupled to the generator (10) via a pair of

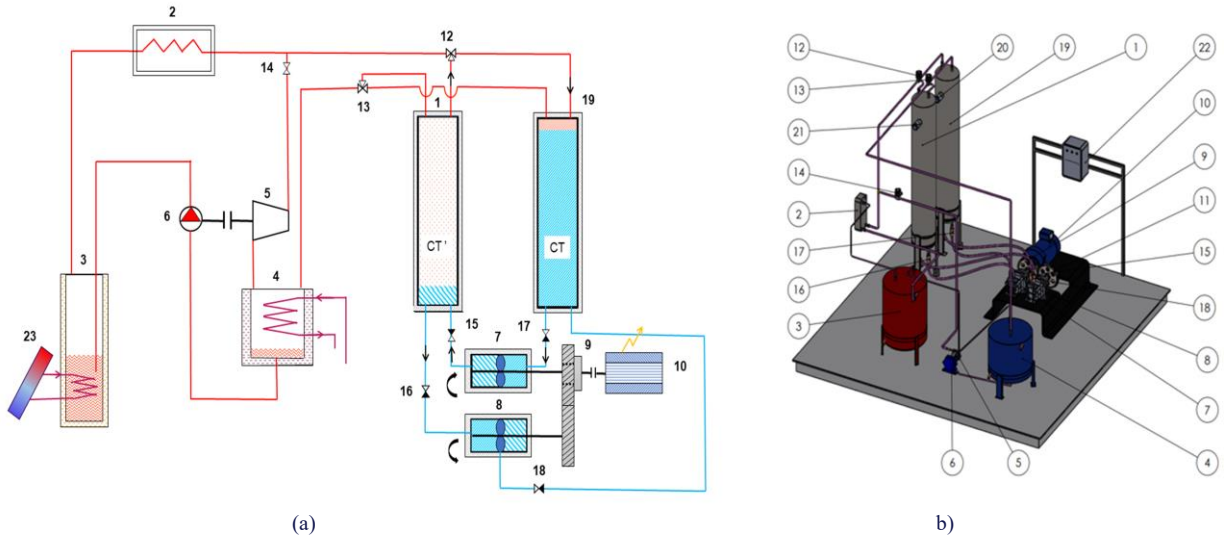

Fig. 1. (a) Schematic and (b) 3D drawing of the novel ORPILI thermo-hydraulic machine : (1) − work-transfer cylinder CT', (2) − superheater, (3) − evaporator, (4) − condenser, (5) − steam turbine, (6) − transfer pump, (7) and (8) − hydraulic motors, (9) − gear, (10) − generator, (11) − gear, (12) and (13) − 2 way solenoid valve, (14) − extraction steam valve, (15)−(18) − non-return valves, (19) − work-transfer cylinder CT, (20) and (21) − level sensor, (22) − panel board, (23) − solar collector.

gears (9) and (11) and the freewheel. Then, the hydraulic oil exits the hydraulic motor (8), passes through the non-return valve (18), and enters the work transfer cylinder (19). The liquid piston then pushes the working fluid steam towards the condenser (4) via the solenoid valve (13). Once the FLP has reached the designated level, which is detected by the level sensor (21), the solenoid valves (12) and (13) are activated, and the cycle begins again.

2.3. Description of the thermodynamic cycle

The operation of the proposed system's ORPILI cycle involves two half cycles, where the roles of the work-transfer cylinders are alternated. The working fluid follows the thermodynamic cycle denoted as (1-2-3-4-5), illustrated schematically in Mollier's *p-h* diagram (pressure vs. enthalpy) in Fig. 2, depicting the fundamental processes and heat transfers within the system. This novel machine operates on a Rankine-type cycle using superheated steam, with a steam generator operating at high pressure and temperature (T_{evap}, p_{evap}), and a condenser operating at low pressure and temperature (T_{cond}, p_{cond}).

The working fluid undergoes four processes: compression, evaporation, expansion, and condensation in sequence to complete a cycle.

The liquid-phase working fluid at low-pressure p_l at state **1** is directed into the pump, where it is isentropically compressed to match the operating pressure of the evaporator at state **2** at high pressure p_h. The pump operates without any heat transfer occurring around it.

2→4: Isobaric heat addition. The working fluid enters the evaporator as a compressed liquid at state **2** and leaves as a superheated vapor at state **4**.

4→5: Isentropic expansion. The superheated vapour at state **4** exits the evaporator and enters the CT, where it undergoes isentropic expansion. The pressure and the temperature of vapour drop during this process to the values at state **5**. During this process, the vapour displaces the transfer liquid (LT) towards the CT' until the liquid reaches the high level.

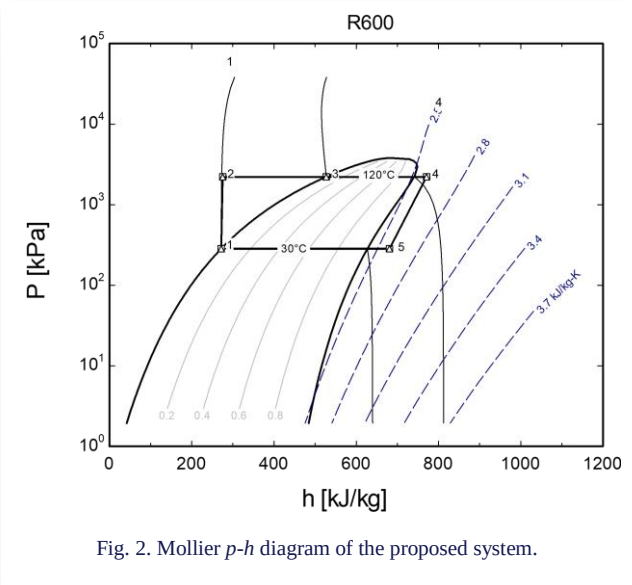

Fig. 2. Mollier *p-h* diagram of the proposed system.

5→1: Isobaric heat rejection in the condenser. The vapour displaced from the CT' during the previous process undergoes isobaric condensation in the condenser.

The performance analysis of the ORPILI thermodynamic cycle for various working fluids is carried out using the mathematical model presented in the next section.

3. Thermodynamic analysis

The ORPILI thermo-hydraulic machine proposed in this study operates within the following temperature ranges: superheating temperatures range from 65°C to 130°C, while evaporation occurs between 60°C and 120°C. However, the temperature at the condenser remains constant at 30°C. These temperature ranges were chosen to evaluate the thermodynamic efficiencies of the machine when using different working fluids.

In this context, various refrigerants are used in low-temperature applications to meet specific performance and environmental criteria, including HFC such as R134a, R152, and others. These refrigerants are harmless to the ozone layer, as they possess a zero ozone depletion potential (ODP) due to the absence of chlorine atoms [22]. Furthermore, HFCs have been subject to regulations under the Kyoto Protocol and the European F-Gas Regulation, aiming to gradually phase out their use by 2030. This is due to their high global warming potential (GWP), which exceeds 150 [23].

Compared to chlorofluorocarbons (CFCs), hydrochlorofluorocarbons (HCFCs) and HFCs, hydrocarbon-based refrigerants (HC) offer a more environmentally friendly alternative. They have a negligible impact on ozone depletion (ODP = 0) and exhibit a minimal potential for contributing to global warming (GWP ≈ 20). However, it should be noted that these refrigerants are highly flammable, necessitating stringent safety measures in both production and usage. Certain hydrocarbons, such as R600a (butane), find application in limited amounts in domestic refrigeration systems, such as household refrigerators [22].

Lastly, hydrofluoroolefin (HFO) gases such as R1234yf, R1234ze, R1233zd, etc. are considered as a new generation of refrigerants (4th generation) and are intended to replace older refrigerants like freons (R134a and R32) in various refrigeration engineering applications (refrigeration, heat pumps, air conditioning, automotive air conditioning, etc.) [23].

Taking into account the aforementioned arguments, the following working fluids are adopted and evaluated for the present ORPILI cycle: R600a, R600, R1234yf, R1234ze, R1233zd, and SES36.

In the thermodynamic analysis, the inputs and outputs of the condensate pump are characterised by the enthalpies h_1 and h_2, respectively, which are dependent on temperature and pressure.

The fluid state at the turbine inlet can be specified by the evaporating pressure and superheat degree. Using CoolProp library [24], parameters such as specific enthalpy and entropy can be calculated. The mathematical equations employed for the thermodynamic analysis of the ORPILI cycle, as detailed in Subsection 2.3, together with the thermal and second law efficiencies, are presented in Table 1. The work performed by the

Table 1. Formulas for ORPILI system.

Item	Thermodynamic formula	No.
Pump work	$W_{pump} = (h_2 - h_1) = v_1(p_2 - p_1)$	(1)
Turbine work	$W_{turbine} = y(h_4 - h_5)$	(2)
Energy balance	$W_{turbine} = W_{pump}$ $y(h_4 - h_5) = (h_2 - h_1)$ $y = \frac{(h_2 - h_1)}{(h_4 - h_5)}$	(3) (4) (5)
Expansion work	$W_{exp} = (1 - y)(h_4 - h_5)$	(6)
Net work developed by the cycle	$W_{cycle} = W_{exp} - W_{pump}$	(7)
Thermal efficiency of the cycle	$\eta_{th} = \frac{W_{cycle}}{Q_{in}} = \frac{\left((1 - y)(h_4 - h_5)\right) - (h_2 - h_1)}{(h_4 - h_2)}$	(8)
2nd law efficiency	$\eta_{II} = \frac{\eta_{th}}{\eta_{Carnot}}$	(9)

pump is given by Eq. (1), while the work generated by the turbine is expressed in Eq. (2). The system's energy balance, outlined in Eqs. (3) and (4), allows for the calculation of the steam extraction ratio, as shown in Eq. (5). The specific expansion work is defined by Eq. (6), whereas the net specific work of the cycle is determined by Eq. (7). The thermal efficiency of the cycle (Eq. (8)) is calculated by the ratio of the net specific work to the specific heat input, while the second law efficiency given by Eq. (9) is used to assess the system's performance relative to the ideal thermodynamic process.

4. Results and discussion of the thermodynamic analysis

The variations in thermal (η_{th}) and second law (η_{II}) efficiencies for the six refrigerants are shown in Table 2, which is, in fact, the synthesis of the results of several previous calculations. These calculations involved determining the thermal and second law efficiencies for various superheat temperatures, each time the evaporation temperature (T_{evap}) was fixed. The superheat temperature was varied within the range of T_{evap} + 5°C to 130°C. Within this range, the thermal and second law efficiencies were calculated. The retained values correspond to the maximum efficiencies.

It is evident from this table that the thermodynamic cycle of the novel ORPILI thermo-hydraulic machine operating with the refrigerants R1234yf and R1234ze develops lower thermal efficiencies compared to other fluids, equal to 11.6% and 13.9 %, respectively. This indicates that these working fluids are not suitable for this type of machine.

Furthermore, the machine achieves optimal performance within the temperature range of 65°C to 120°C when using refrigerants R600a, R600, R1233zd, and SES36. Among these, the maximum thermal efficiencies recorded are 16.1%, 16.9%, 17.5%, and 15.6%, respectively.

The thermal efficiency (η_{th}) reaches a maximum value of 17.5% with the refrigerant R1233zd at a superheat temperature (T_{sc}) of 130°C, matching to a second law efficiency (η_{II}) equal to 78.7%. The corresponding Carnot efficiency and pressure drops are about 22.4% and 1416.4 kPa, respectively (Fig. 3). Based on the aforementioned selection criteria, the results suggest that R1233zd fluid is the most suitable.

The hydrofluoroolefin gas R1233zd is identified as the most suitable working fluid for CAPILI applications, serving as a re-

Table 2. Thermal and second law efficiencies according to the superheated temperature.

T_{sc} (°C)	R600a		R600		SES36		R1233zd		R1234ze		R1234yf	
	η_{th}	η_{II}	η_{th}	η_{II}	η_{th}	η_{II}	η_{th}	η_{II}	η_{th}	η_{II}	η_{th}	η_{II}
65	0.078	0.871	0.080	0.888	0.072	0.799	0.081	0.903	0.077	0.852	0.073	0.817
70	0.089	0.855	0.090	0.873	0.082	0.789	0.092	0.889	0.086	0.833	0.082	0.795
75	0.098	0.839	0.100	0.859	0.091	0.779	0.102	0.877	0.095	0.815	0.090	0.773
80	0.107	0.824	0.109	0.846	0.099	0.769	0.112	0.864	0.103	0.797	0.097	0.752
85	0.115	0.809	0.118	0.832	0.107	0.759	0.121	0.852	0.110	0.779	0.103	0.729
90	0.122	0.7941	0.126	0.819	0.115	0.748	0.129	0.840	0.117	0.760	0.109	0.707
95	0.129	0.780	0.133	0.807	0.122	0.739	0.137	0.829	0.123	0.743	0.113	0.683
100	0.135	0.767	0.140	0.794	0.129	0.728	0.144	0.817	0.127	0.724	0.116	0.699
105	0.141	0.752	0.147	0.782	0.135	0.718	0.151	0.806	0.132	0.704	–	–
110	0.147	0.739	0.153	0.770	0.141	0.709	0.158	0.796	0.136	0.683	–	–
115	0.152	0.725	0.158	0.758	0.146	0.699	0.164	0.785	0.139	0.698	–	–
120	0.156	0.711	0.164	0.746	0.151	0.689	0.170	0.774	–	–	–	–
125	0.159	0.698	0.164	0.747	0.156	0.679	0.175	0.764	–	–	–	–
130	0.161	0.702	0.169	0.736	0.155	0.676	0.175	0.766	–	–	–	–

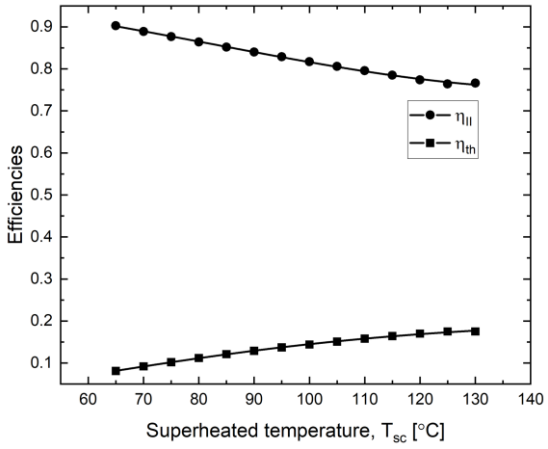

Fig. 3. Variation of efficiencies (η_{th}, η_{II}) with the superheated temperature of R1233zd as the working fluid.

placement for R123, which was previously extensively utilized in organic Rankine cycle (ORC) applications. In addition, R1233zd has a limited environmental impact, is completely non-flammable, and is non-toxic [25].

5. Hydraulic analysis

In this section, mathematical modelling of the hydraulic part of the novel ORPILI thermo-hydraulic machine configuration is addressed. This aspect of the study highlights the originality of the proposed concept. Based on the calculations carried out and the selection of the suitable working fluid R1233zd for this system application, a series of analyses have been developed to study the behaviour of the hydraulic system (Fig. 4) within the new proposed cycle with the fluid R1233zd. These analyses demonstrate the impact of changes on the overall cycle, particularly with variations in temperatures: T_{sc} = 65−130°C, T_{evap} = 60−120°C, and T_{cond} = 30°C.

Hence, two operating cases are highlighted and analysed. The first one corresponds to the operating regime with a maximum value of thermal efficiency η_{th_max} = 17.5% and pressure drop equal Δp = 1416.4 kPa, while the second case corresponds to the operating regime with a maximum value of second law efficiency η_{II_max} = 90.25% and a pressure drop Δp = 235.3 kPa. However, in both cases, the total height corresponding to the height between the transfer liquid levels in transfer cylinders is adopted equal to $\Delta H = (H_1 - H_2)$ = 0.1 m (Fig. 4). This hypothesis is demonstrated later. Finally, the density of the transfer liquid is adopted equal to ρ = 900 kg/m³.

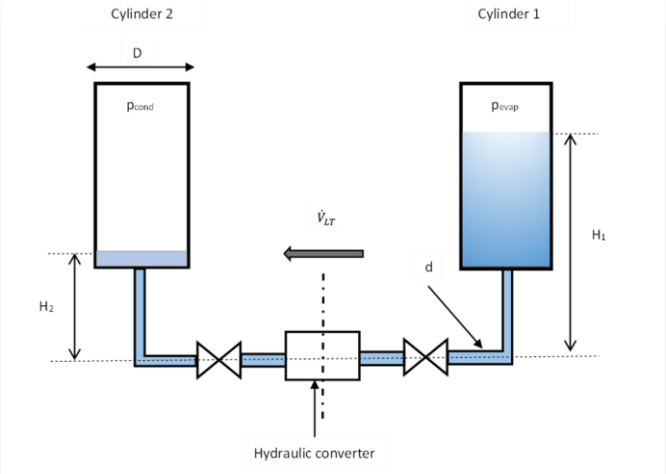

Fig. 4. Hydrostatic scheme of the hydraulic part of the power plant [20]; H_1 and H_2– heights relative to the reference plane, $\dot{V}_{LT}$ – flow rate.

5.1. Mathematical modelling

Figure 4 illustrates the transfer of the liquid (LT) from one cylinder to another, passing through the hydraulic converter and valves. The valves control the flow of the transfer liquid in and out of the hydraulic converter, respectively.

Table 3. Mathematical formulations used in hydraulic analysis.

Formula	
$p_{evp} + \frac{\rho V_1^2}{2} + \rho g H_1 = p_{cond} + \frac{\rho V_2^2}{2} + \rho g H_2 + \frac{P_{hyd}}{\dot{V}_{LT}} + \Delta P_{minor\_losses}$	(10)
$P_{hyd} = -\frac{8\rho K_{total}\dot{V}_{LT}^3}{\pi^2 d^4} + (\Delta p + \Delta H \rho g)\dot{V}_{LT}$	(11)
$K_{total} = 2K_{vs}d + K_{entrance} + 2K_{elbow} + K_{exit}$	(12)
$\frac{8\rho K_{total}\dot{V}_{LT}^3}{\pi^2 d^4} - (\Delta p + \Delta H \rho g)\dot{V}_{LT} + P_{hyd} = 0$	(13)
$\dot{V}_{LT}^3 - C_1\dot{V}_{LT} + C_2 = 0$	(14)
$C_1 = \frac{(\Delta p + \Delta H \rho g)g\pi^2 d^4}{8K_{total}}$	(15)
$C_2 = \frac{P_{hyd} g\pi^2 d^4}{8K_{total}}$	(16)
$\Delta \leq 0 \rightarrow \frac{C_2^2}{4} - \frac{C_1^3}{27} \leq 0$ [14]	(17)
$\frac{\left(\frac{P_{hyd} g\pi^2 d^4}{8K_{total}}\right)^2}{4} \leq \frac{\left[\frac{(\Delta p + \Delta H \rho g)g\pi^2 d^4}{8K_{total}}\right]^3}{27}$	(18)
$K_{total} \leq \frac{\pi^2 d^4 (\Delta p + \Delta H \rho g)^3}{54\rho P_{hyd}^2}$	(19)
$P_{available} = \Delta p \frac{\pi D^2}{4}\Delta H f = \Delta p \frac{\pi D^2}{4}\frac{\Delta H}{\tau}$	(20)
$P_{admissible} = P_{hyd}\dot{V}_{LT\_admissible}$	(21)
$\dot{V}_{LT\_admissible} = V_{admissible}\pi\frac{d^2}{4}$	(22)
$\mathrm{Re}_{admissible} = \frac{V_{admissible} d}{\sigma}$	(23)
$K_{total\_min} = K_{total} P_{available} = \frac{\pi^2 d^4 (\Delta p + \Delta H \rho g)^3}{54\rho P_{available}^2}$	(24)
$K_{total\_max} = K_{total} P_{admissible} = \frac{\pi^2 d^4 (\Delta P_t)^3}{54\rho P_{available}^2}$	(25)
$\dot{V}_{LT} = \pi d^2 \sqrt{\frac{\Delta P_t}{8\rho K_{total}}}$	(26)
$\dot{V}_{LT\_min} = \dot{V}_{LT} K_{total\_min}$	(27)
$\dot{V}_{LT\_max} = \dot{V}_{LT} K_{total\_max}$	(28)

In order to make the analysis smooth and clear, the following definitions are imperative (as detailed in Table 3). Hydraulic power denoted as P_{hyd}, is defined as the power consumed by the hydraulic converter, Eq. (11). It can be determined by utilizing the Bernoulli equation, Eq. (10), and taking into account the minor losses characterized by their flow coefficient. These los-ses occur in various circumstances such as entry to a pipe from a tank, exit from a pipe into a tank, bends in a pipe, valves, and so forth (Fig. 4). The total flow coefficient (K_{total}) of the abovementioned minor losses is determined using Eq. (12). The values of loss coefficients for the threaded elbow (K_{elbow}), the entry to a pipe from a cylinder ($K_{entrance}$), and the exit from a pipe into cylinder (K_{exit}) can be found in [26]. Moreover, the loss coefficient of the valves (K_{vs}) which is related to the nominal diameter is determined based on [27].

In fact, the hydraulic analysis was carried out using Bernoulli's equation between two points located in the evaporator and condenser. The purpose of this analysis at this stage is to size the hydraulic circuit, specifically to define the diameter d based on the hydraulic power consumed by the hydraulic converter. By assuming a constant pressure difference (Δp), a maximum value of hydraulic power is obtained, which allows for determining the maximum diameter (d) of the circuit.

Even when assuming a constant pressure difference to estimate the hydraulic power, the thermal (Eq. (8)) and second law (Eq. (9)) efficiencies are not affected by this assumption. The efficiencies in question were calculated from the net specific work of the thermodynamic cycle, Eq. (7).

However, it would also have been possible to calculate the available mechanical power ($P_{available}$) defined as the mechanical power imparted by the engine cycle to the transfer liquid, from the net work of the cycle (W_{cycle}, Eq. (7)), provided that the mass flow rate of the cycle ($\dot{m}$) was known ($P_{available} = W_{cycle}\dot{m}$). This is equivalent to determining the duration τ of the thermodynamic cycle or its frequency f.

The available mechanical power (Eq. (20)) depends on the diameter of the transfer cylinder, which is set at D = 1 m in this study, the height or vertical distance traversed by the transfer liquid, the pressure differential (Δp), and ultimately, the frequency ($f = 1/\tau$) of a single thermodynamic cycle. At this stage of the study, it is only possible to vary the cycle duration (τ) within a hypothetical range. This power may be transmitted either wholly or partially to the turbine, contingent upon the hydraulic circuit losses (comprising bends, valves, etc.), which, in turn, hinge upon the diameter of the transfer piping and the volumetric flow rate of the transfer liquid. However, a portion of this available mechanical power ($P_{available}$) at the transfer cylinders is expended in overcoming the losses in the hydraulic circuit, deduced directly from Eq. (11). Meanwhile, the remaining is transformed by the hydraulic converter into mechanical power.

Furthermore, among the conditions that must be taken into consideration are the flow velocity limits to maintain the integrity and performance of the system. It emerges that the flow velocity (or admissible speed) can go up to 6 m/s [28], which will considerably increase the admissible power and in return will increase the specific power of the new power plant. In fact, it is a recommended flow velocity for hydraulic pipes to avoid transitioning to the rough turbulent regime.

Under these circumstances, admissible power refers to the maximum allowable power that a hydraulic system or component can handle without exceeding its design limitations or causing damage. The admissible power ($P_{admissible}$, Eq. (21)) can be determined by replacing the admissible speed ($V_{admissible}$) in the hydraulic power (Eq. (11)), taking into account several factors, including the design, materials, and operating circumstances of the hydraulic components.

Also, substituting the admissible speed in the Reynolds number equation gives the admissible Reynolds number ($\mathrm{Re}_{admissible}$, Eq. (23)). Along with the admissible speed ($V_{admissible}$), the admissible Reynolds number is also affected by the kinematic viscosity of the hydraulic fluid (σ).

The selection of the hydraulic oil viscosity grade should align with the typical operating temperature. It is important to remember that viscosity is a measure of the oil's resistance to flow, so in hydraulic systems that are dependent on flow, viscosity is important with respect to both lubrication and energy transmission [29]. According to [29], hydraulic systems normally use oil with a viscosity range of 32–68 cSt at 40°C. However, in a thermo-hydraulic machine where the hydraulic oil comes into contact with the superheated vapour, the choice of the hydraulic oil depends on the temperature of the superheated vapour. For instance, a temperature of 100°C requires a hydraulic oil with a minimum viscosity of 15 cSt, i.e. a hydraulic oil ISO VG 150. At a temperature of 130°C and a viscosity of 15 cSt, the selection of an ISO VG 460 hydraulic oil is necessitated. This requirement can be substantiated through reference to oil viscosity-temperature charts, as documented in sources [30−32]. In this case, the power plant must be started by heating the hydraulic oil to a temperature greater than 40°C so that the kinematic viscosity is less than 600 cSt.

Moreover, finding the flow rate via the turbine is possible by solving the cubic equation (14). The discriminant (Δ) of this cubic equation has to be negative in order to get real solutions [14].

The definition of the maximum value of K_{total} that may be utilized to find real solutions for the flow rate in cubic equation (14) is made possible by inequality (19). Equations (24) and (25) establish the minimum and maximum values of K_{total} at the two powers $P_{admissible}$ and $P_{available}$, respectively.

Finally, to ensure the proper functioning of the turbine, it is necessary for the hydraulic power (Eq. (11)) to be positive. Through this condition, the relation of flow rate can be deduced (Eq. (26)). By substituting the expressions of the minimum and maximum total flow coefficient (Eqs. (24) and (25)) into the equation of flow rate (Eq. (26)), a condition on this flow rate is obtained in Eqs. (27) and (28).

6. Results and discussion of the hydraulic analysis

Figures 5a and 5b illustrate the evolution of hydraulic power for different diameters. They depict the maximum hydraulic powers and optimal flow rates for each diameter. For a given diameter of the hydraulic circuit piping, the shape of the hydraulic power curve is parabolic. Several readings can be inferred from this figure. The power is zero at the two points of intersection of the

curve with the axis representing flow rate. The first point corresponds to the converter's idle state with zero volumetric flow rate. The second point also corresponds to the converter's idle state with maximum volumetric flow rate and maximum pressure losses in the hydraulic circuit. The hydraulic power is maximum for a well-considered value of pressure losses and consequently a well-determined volumetric flow rate. The value of pressure losses at this point can only be minimal. In other words, the pressure losses of the hydraulic circuit, as a function of the volumetric flow rate for a given diameter, can vary from a minimum value when the converter is at rest to their maximum value when the converter is once again at rest (Figs. 5a and 5b). However, for a determined diameter of the hydraulic circuit, the hydraulic power reaches its maximum value, which corresponds to an optimal volumetric flow rate, i.e. minimum pressure losses in the circuit.

To take advantage of this determined maximum hydraulic power for a given diameter, it is necessary for the power available at the transfer cylinder to be greater than or equal to the hydraulic power. This implies that the available mechanical power at the transfer cylinder, which in turn depends on the frequency of the thermodynamic cycle (f) or the duration of a thermodynamic cycle (τ) (Eq. (20)). The latter depends on the temperatures and/or pressures of the hot and cold reservoirs, the working fluid, heat transfer parameters (exchange surfaces, heat transfer coefficient, temperature jumps, etc.). In this case, in the absence of real data and with the aim of completing this analysis, we can assume a frequency for which the available mechanical power at the transfer cylinder is equal to the hydraulic power, represented by the horizontal line passing through the maximum P_{hyd} for a given diameter.

It is observed that the available mechanical power at the transfer cylinder increases with the growth of the frequency of the thermodynamic cycle. This means that the higher the number of cycles per second, the greater the available mechanical power at the transfer cylinder ($P_{available}$).

In the first case (Fig. 5a), with the maximum value of thermal efficiency η_{th_max} = 17.5% and a pressure drop Δp = 1416.4 kPa, the maximum hydraulic power is 5.3 kW for d = 0.02 m. However, it is equal to 0.4 kW for the second case (Fig. 5b) with the maximum value of second law efficiency η_{II_max} = 90.2% and a pressure drop Δp = 235.3 kPa for the same diameter. When the diameter is d = 0.046 m, in both first and second cases, the maximum hydraulic power increases to 27.8 kW and 1.9 kW, respectively. These findings suggest that different types of converters must be selected in each case. For the first case, both the hydraulic turbine and piston-converter are suitable due to the relatively high pressure differential and high hydraulic power. However, for the second case, only a hydraulic turbine is suitable due to the low-pressure differential between the transfer cylinders.

However, it is crucial to emphasize that high mechanical powers can be produced only at the high thermal efficiency operating mode. In contrast, operating modes with high second low efficiencies cannot provide high levels of mechanical powers.

As previously noted, a total height of 0.1 m was selected for ΔH. This decision is supported by the relatively minor influence of ΔH on hydraulic power, as illustrated in Fig. 6. It is clear that ΔH is significantly related to the duration of the thermodynamic cycle (τ), and thus to the frequency (f). Specifically, a slower thermodynamic cycle corresponds to a higher value of ΔH.

The permissible range of flow rates according to the pressure drop in transfer cylinders obtained for both studied cases are shown in Figs. 7a and 7b. They are likewise compared to those obtained by Semmari et al. [14]. Consequently, the resulting working area built according to the minimum and maximum total flow coefficients is identical to the one obtained by Semmari et al. [14] for their thermo-hydraulic machine. Nonetheless, in

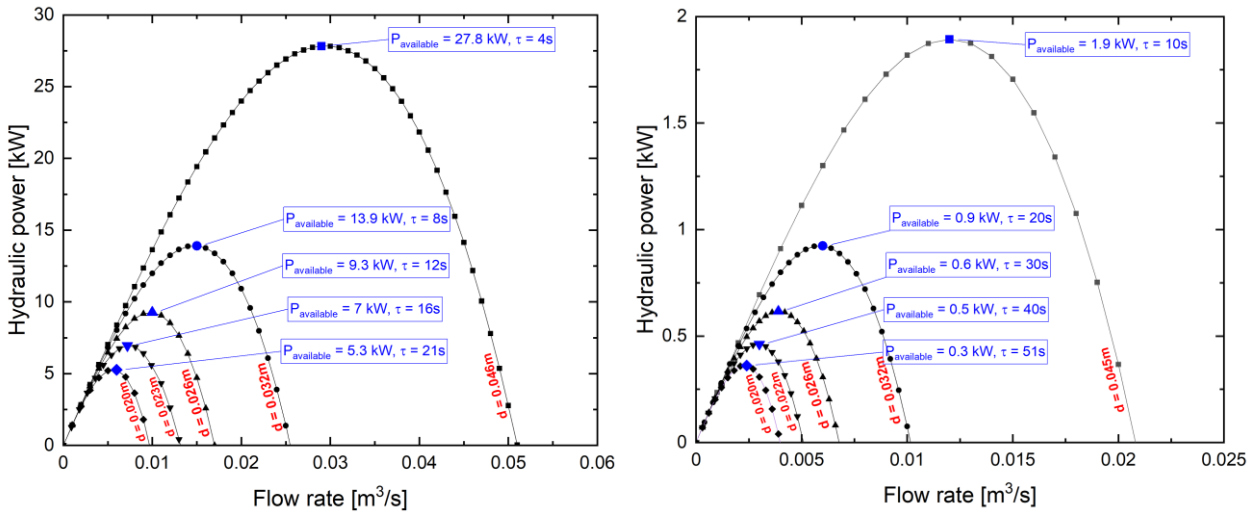

(a) (b)

Fig. 5. Variation of the hydraulic power according to the volume flow rate: (a) case 1 − Δp = 1416.4 kPa and η_{th_max} = 17.5%, (b) case 2 − Δp = 235.3 kPa and η_{II_max} = 90.25%.

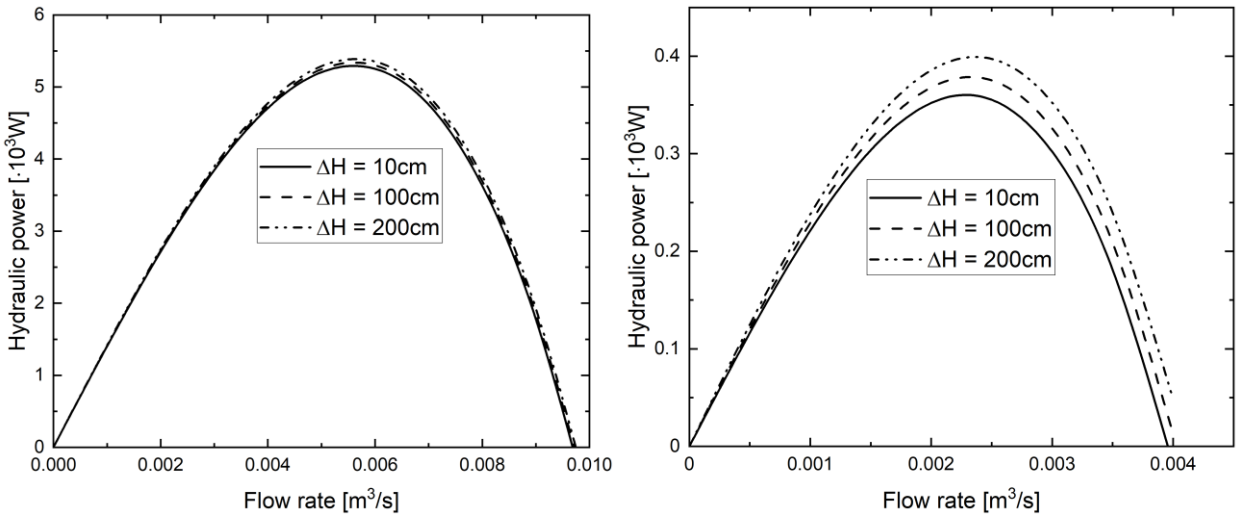

Fig. 6. Variation of the hydraulic power with the flow rate and the total height ΔH for d = 0.02 m: (a) case 1 − Δp = 1416.4 kPa and η_{th_max} = 17.5%, (b) case 2 − Δp = 235.3 kPa and η_{II_max} = 90.25%.

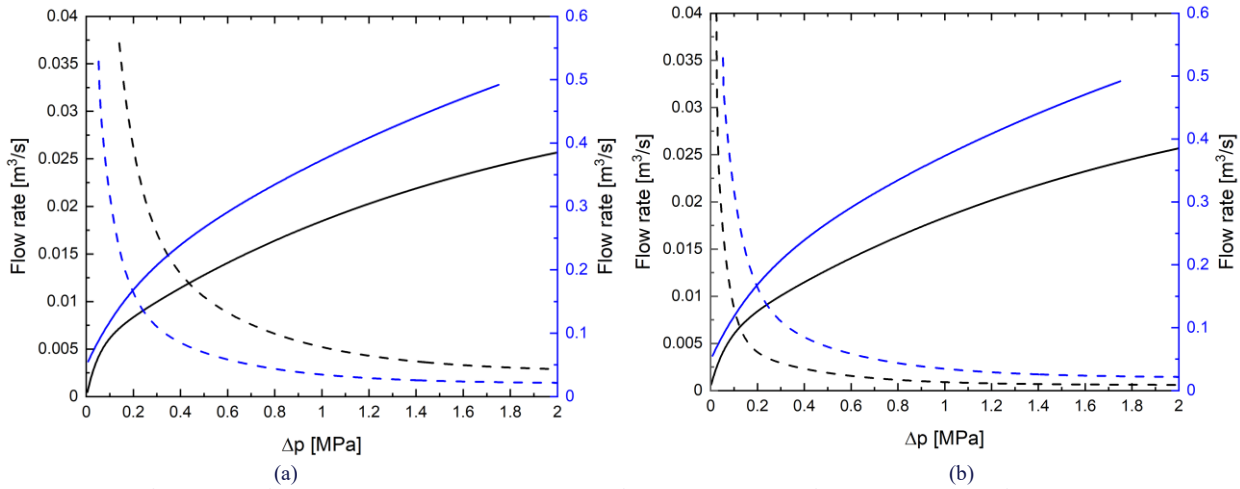

Fig. 7. Comparison of the allowed flow rates according to the pressure drop for d = 0.03 m in transfer cylinders obtained for both studied cases with those obtained by Semmari et al. [14]: — flow rate (K_{total_min}) for the present study, — flow rate max studied by Semmari et al. [14], - - flow rate (K_{total_max}) for the present study, - - flow rate min studied by Semmari et al. [14].

the aforementioned work, flow rates seem to be a little bit overrated. To clarify the disparity in flow rates ranges, the homogeneity of the hydraulic power expression provided by Semmari et al. was checked through a dimensional analysis. It appears that the term containing the loss coefficient looks to have a unit of m^3/s when it should really be expressed in watts!

As previously mentioned, solving Eq. (14) enables the determination of the flow rate through the turbine that satisfies the condition $\dot{V}_{LT\_min} < \dot{V}_{LT} < \dot{V}_{LT\_min}$. The set of retained solutions for flow rates and pressure drops is located between the two curves. This information is valuable when comparing various gases and operating regimes. It is clear that, as you move to the left (i.e. with decreasing pressure drop), the range of flow rates narrows. Conversely, moving to the right broadens the range of flow rates.

Admissible powers and admissible Reynolds numbers versus diameter are depicted in Table 4 for cases 1 and 2 at the admissible speed $V_{admissbile}$ of 6 m/s. It can be observed that in case 1 the admissible power increases from 2.6 kW to 574.5 kW as the diameter increases. Similarly, for case 2 the admissible power increases from 0.3 kW to 73.6 kW as the diameter increases. The hydraulic system can accommodate higher power levels, suggesting that a larger diameter enables better fluid flow and can meet higher power demands. However, it is important to ensure that the power is not simultaneously exceeded in a hydraulic system. Operating at excessive admissible power levels can lead to increased wear, pressure drops, and potential system failures.

Additionally, the Reynolds number in Table 4 increases at the admissible speed as the diameter increases, ranging from 8 000 to 120 000 for cases 1 and 2, respectively. This increase in the Reynolds number at the admissible speed indicates a transition from a smooth turbulent regime, characterized by a Reynold number ranging between 2 300 and 100 000 [26]. Hence, the obtained results show that in both cases when the pipe diameter

Table 4. Variations of admissible and available mechanical powers and Reynold numbers according to diameters.

Case 1			
Δp = 1416.4 kPa corresponding to η_{th_max} = 17.5%			
d (m)	$P_{admissible}$(kW)	$Re_{admissible}$	$P_{available}$ (kW)
0.02	2.6	8000	5.3
0.03	5.8	12000	11.9
0.04	10.3	16000	21.2
0.05	16.1	20000	33.0
0.06	23.1	24000	48.4
0.07	31.5	28000	64.3
0.08	14.2	32000	84.3
0.10	64.2	40000	130.9
0.125	100.3	50000	203.7
0.15	144.3	60000	292.8
0.20	256.1	80000	505.7
0.25	399.6	100000	778.0
0.30	574.5	120000	1101.5

Case 2			
Δp = 235.3 kPa corresponding to η_{II_max} = 90.25%			
d (m)	$P_{admissible}$(kW)	$Re_{admissible}$	$P_{available}$ (kW)
0.02	0.3	8000	0.4
0.03	0.8	12000	0.8
0.04	1.4	16000	1.4
0.05	2.1	20000	2.3
0.06	3.1	24000	3.2
0.07	4.2	28000	4.4
0.08	5.5	32000	5.7
0.10	8.5	40000	8.9
0.125	13.3	50000	13.8
0.15	19.1	60000	19.9
0.20	33.5	80000	34.5
0.25	51.7	100000	53.0
0.30	73.6	120000	74.8

remains under 0.25 m, the flow regime is still far from the rough turbulent regime.

Another careful reading from Table 4 allows to underline another established fact when comparing the available and admissible powers. The available power exceeds the admissible one by an average value of 51% and 4%, respectively for the two cases. This suggests that the operating regime with a maxi-mum value of second law efficiency η_{II_max} = 90.25% (case 2) is able to convert all the available power at the transfer cylinders more efficiently than the one with a maximum value of thermal efficiency η_{th_max} = 17.5% (case 1). However, the only drawback is that a power plant operating according to case 2 cannot provide high levels of mechanical powers and have a relatively low specific power.

7. Conclusions

In summary, this work examines a unique ORPILI thermo-hydraulic machine that was first conceived by the Research Laboratory in Engineering, Materials and Structures. The study is thought of as a multi-aspect optimization of the new concept of a power plant and it is divided into two primary sections: thermodynamic and hydraulic analysis. Hence, the following major conclusions are drawn based on the obtained results:

- Among several suggested working fluids, the thermodynamic analysis has shown that the R1233zd is the most appropriate for mechanical power generation from low temperature reservoirs. It is demonstrated that thermal and second law efficiencies can reach maximum values of 17.5% and 90.3%, respectively. However, high mechanical powers can be produced only at high thermal efficiencies operating mode. On the other hand, operating modes with high second low efficiencies cannot provide high levels of mechanical powers.
- For a given diameter of the hydraulic circuit piping, the shape of the hydraulic power curve is parabolic. However, the hydraulic power reaches its maximum value, which corresponds to minimum pressure losses in the circuit, i.e. the optimal volumetric flow rate.
- It is shown that there is a certain operating area with allowed values of flow rate and pressure drop in transfer cylinders. The boundaries of this area are determined by the minimum and maximum values of the total flow coefficients.
- A power plant operating with a maximum value of second law efficiency cannot provide high levels of mechanical powers and have a relatively low specific power. To develop a significant power, it will be necessary to opt for a power plant operating with a maximum value of thermal efficiency, i.e. relatively high specific power.

The last conclusion aligns with several postulates of the second law of thermodynamics. It evokes the initial observation made by Nicolas Leonard Sadi Carnot during his analysis of steam engines, when he realized that there was a fundamental limit to the amount of work generated from a given amount of heat. In light of this, more studies will need to be done. Their primary focus will be on the transfer cylinders and the mechanical gearbox with the freewheel.

References

[1] Shah, Y.T. (2022). *Advanced power generation systems: Thermal sources* (1st ed.). CRC Press. doi: 10.1201/9781003328087

[2] Yilmaz, F. (2019). Energy, exergy and economic analyses of a novel hybrid ocean thermal energy conversion system for clean power production. *Energy Conversion and Management*, 196, 557–566. doi: 10.1016/j.enconman.2019.06.028

[3] Khaligh, A., & Onar, O.C. (2010). *Energy harvesting: Solar, wind, and ocean energy conversion systems*. CRC Press. doi: 10.1201/9781439815090

[4] Tong, W. (2010). Fundamentals of wind energy. *WIT Transactions on State of the Art in Science and Engineering*, 44, 3–48. doi: 10.2495/978-1-84564-205-1/01

[5] Igwe, C.I. (2021). Geothermal energy: A review. I*nternational Journal of Engineering Research & Technology*, 10(3). doi: 10.17577/IJERTV10IS030164

[6] Benti, N.E., Gurmesa, G.S., Argaw, T., Aneseyee, A.B., Gunta, S., Kassahun, G.B., Aga, G.S., & Asfaw, A.A. (2021). The current status, challenges and prospects of using biomass energy in Ethiopia. *Biotechnology for Biofuels*, 14(1), 209. doi: 10.1186/s13068-021-02060-3

[7] Pan, Y., Yang, F., Zhang, H., Yan, Y., Yang, A., Liang, J., & Yu, M. (2022). Performance prediction and working fluid active design of organic Rankine cycle based on molecular structure. *Energies*, 15(21), 8160. doi: 10.3390/en15218160

[8] Pan, L., & Wang, H. (2013). Improved analysis of organic Rankine cycle based on radial flow turbine. *Applied Thermal Engineering*, 61(2), 606−615. doi: 10.1016/j.applthermaleng.2013.08.019

[9] Humphrey, H.A. (1909). An internal-combustion pump, and other applications of a new principle. *Proceedings of the Institution of Mechanical Engineers*, 77(1). doi: 10.1243/PIME_PROC_1909_077_019_02

[10] Van de Ven, J.D., & Li, P.Y. (2009). Liquid piston gas compression. *Applied Energy*, 86(10), 2183−2191. doi: 10.1016/j.apenergy.2008.12.001

[11] Van de Ven, J.D. (2009). Mobile hydraulic power supply: Liquid piston Stirling engine pump. *Renewable Energy*, 34(11), 2317−2322. doi: 10.1016/j.renene.2009.01.020

[12] Motamedi, M., Ahmadi, R., & Jokar, H. (2018). A solar pressurizable liquid piston stirling engine: Part 1, mathematical modeling, simulation and validation. *Energy*, 155, 796−814. doi: 10.1016/j.energy.2018.05.002

[13] Ahmadi, R., Jokar, H., & Motamedi, M. (2018). A solar pressurizable liquid piston stirling engine: Part 2, optimization and development. *Energy*, 164, 1200−1215. doi: 10.1016/j.energy.2018.08.197

[14] Semmari, H., Stitou, D., & Mauran, S. (2012). A novel Carnot-based cycle for ocean thermal energy conversion. *Energy*, 43(1), 361−375. doi: 10.1016/j.energy.2012.04.017

[15] Mauran, S., Martins, M., Stitou, D., & Semmari, H. (2012). A novel process for engines or heat pumps based on thermal-hydraulic conversion. *Applied Thermal Engineering*, 37, 249–257. doi: 10.1016/j.applthermaleng.2011.11.026

[16] Stitou, D. (2013). *Transformation, Conversion, Stockage, Transport de l'énergie thermique par procédés thermochimiques et thermo-hydrauliques*. Habilitation à Diriger des Recherches en Énergétique − Génie des Procédés, Université de Perpignan. https://tel.archives-ouvertes.fr/tel-00841655

[17] Borgogno, R., Mauran, S., Stitou, D., & Marck, G. (2017). Thermal-hydraulic process for cooling, heating and power production with low-grade heat sources in residential sector. *Energy Conversion and Management*, 135, 148–159. doi: 10.1016/j.enconman.2016.12.064

[18] Semmari, H., Mauran, S., & Stitou, D. (2017). Experimental validation of an analytical model of hydraulic motor operating under variable electrical loads and pressure heads. *Applied Energy*, 206, 1309–1320. doi: 10.1016/j.apenergy.2017.10.010

[19] Zebbar, D., Guelib, A., Kherris, S., Zebbar, S., Mostefa, K., & Kaddouri, N. (2019). Thermodynamic study and analysis of thermohydraulic cycle for power generation. *Recueil de mécanique*, 3(2), 299−305 (in French). doi: 10.5281/zenodo.2581463

[20] Semmari, H. (2012). *Production d'électricité par procédé thermo-hydraulique. Application à l'exploitation de l'énergie thermique des mers*. Thése de doctorat, Université de Perpignan (in French).

[21] Zebbar, D., Guelib, A., Rahmani, Z., Zebbar, S., & Kherris, S. (2022). *Machine thermohydraulique pour la production continue de puissance mécanique avec piston liquide fonctionnant suivant le cycle de Rankine*, Algeria. Patent No. 220156.

[22] Martins, M. (2010). *Nouveau procédé thermo-hydraulique appliqué au rafraîchissement solaire de l'habitat. Analyse et optimisation thermodynamiques*.Thèse de doctorat, Université de Perpignan (in French).

[23] Maalem, Y., Madani, H., & Mehemmai, M. (2023). Modélisation mathématique et simulation numérique des performances de refroidissement de différentes unités de réfrigération à compression de vapeur: application de nouveaux fluides frigorigènes. *Revue des Sciences et Science de l'ingénieur*, 10 (1), 21−39 (in French).

[24] Bell, I.H., Wronski, J., Quoilin, S., & Lemort, V. (2014). Pure and Pseudo-pure fluid thermophysical property evaluation and the open-source thermophysical property library CoolProp. *Industrial & Engineering Chemistry Research*, 53(6), 2498–2508. doi: 10.1021/ie4033999

[25] Borgogno, R. (2017). Procédé thermo-hydraulique solaire appliqué à la trigénération dans le secteur résidentiel. Thése de doctorat, Université de Perpignan (in French). https://tel.archives-ouvertes.fr/tel-01620245

[26] Çengel, Y.A., & Cimbala, J.M. (2006). *Fluid mechanics: Fundamentals and applications*. McGraw-Hill Higher Education.

[27] Regin. *GF2/GF3 Rev. C 2– and 3–way DIN-standard flanged valve*. https://www.regincontrols.com/globalassets/pimmedia-files/documents/gf2_gf3_ps10097_en.pdf [accessed 7 Jul. 2024].

[28] Savić, V., Knežević, D.M., Lovrec, D., Jocanović, M., & Karanović, V. (2009). Determination of pressure losses in hydraulic pipeline systems by considering temperature and pressure. *Strojniški vestnik − Journal of Mechanical Engineering*, 55(4), 237−243 UDC 621.643

[29] Pirro, D.M., Wessol, A.A., & Wills, J.G. (2001). *Lubrication fundamentals* (2nd ed.). CRC Press.

[30] Oil viscosity/temperature chart. OEM Dynamics. https://oemdynamics.us/documents/InstructionBooks/viscosity.pdf [accessed 7 Jul. 2024].

[31] Majumdar, S.R. (2003). Oil hydraulic systems: Principles and maintenance. McGraw-Hill.

[32] Chapple, P. (2002). Principles of hydraulic system design (1st ed.). Coxmoor Publishing Company.